Plasmonic Cu Nanoparticles for the Low-temperature Photo-driven Water-gas Shift Reaction

Jiaqi Zhao[+], Ya Bai[+], Zhenhua Li, Jinjia Liu, Wei Wang, Pu Wang, Bei Yang, Run Shi, Geoffrey I. N. Waterhouse, Xiao-Dong Wen, Qing Dai, and Tierui Zhang**

Abstract: The activation of water molecules in thermal catalysis typically requires high temperatures, representing an obstacle to catalyst development for the low-temperature water-gas shift reaction (WGSR). Plasmonic photocatalysis allows activation of water at low temperatures through the generation of light-induced hot electrons. Herein, we report a layered double hydroxide-derived copper catalyst (LD-Cu) with outstanding performance for the low-temperature photo-driven WGSR. LD-Cu offered a lower activation energy for WGSR to H_2 under UV/Vis irradiation (1.4 $W cm^{-2}$) compared to under dark conditions. Detailed experimental studies revealed that highly dispersed Cu nanoparticles created an abundance of hot electrons during light absorption, which promoted $*H_2O$ dissociation and *H combination via a carboxyl pathway, leading to the efficient production of H_2. Results demonstrate the benefits of exploiting plasmonic phenomena in the development of photo-driven low-temperature WGSR catalysts.

Introduction

Hydrogen (H_2) is a very promising energy carrier, widely considered the logical successor to fossil fuels for transportation and electricity generation.[1] The water-gas shift reaction (WGSR, $CO+H_2O \rightarrow CO_2+H_2$) is an indispensable catalytic process in today's chemical industry for H_2 production. The WGSR is thermodynamically favored at low temperatures, but generally requires high temperatures ($>300\,^{\circ}C$) when using catalysts based on earth-abundant elements (e.g. Cu-based catalysts and Fe-based catalysts) due to kinetic limitations associated with such catalysts.[2] With a view towards lowering the energy input of H_2 production, researchers are now actively seeking catalysts for the low-temperature WGSR, which requires the discovery of strategies capable of efficiently activating water at low temperatures (operating temperatures below $250\,^{\circ}C$).[3] Recently, Ma et al. reported that noble-metal Au clusters and Pt_1–Pt_n clusters on α-MoC delivered excellent low-temperature WGSR activity, obtaining record-breaking H_2 production rates.[2a,4] Whilst impressive, the use of noble metals to thermally drive the low-temperature WGSR is not viable for industrial scale H_2 manufacture due to high capital costs and massive heat energy input supplied electrically or through the combustion of fossil fuels. Therefore, the design and development of non-noble metal catalysts capable of activat-

[*] J. Zhao,[+] Z. Li, P. Wang, Dr. R. Shi, Prof. T. Zhang
Key Laboratory of Photochemical Conversion and Optoelectronic Materials, Technical Institute of Physics and Chemistry, Chinese Academy of Sciences
Beijing 100190 (China)
E-mail: lizhenhua@mail.ipc.ac.cn
tierui@mail.ipc.ac.cn

J. Zhao,[+] P. Wang, Prof. Q. Dai, Prof. T. Zhang
Center of Materials Science and Optoelectronics Engineering, University of Chinese Academy of Sciences
Beijing 100049 (China)

Y. Bai[+]
State Key Laboratory of Chemical Resource Engineering, Beijing Advanced Innovation Center for Soft Matter Science and Engineering, Beijing University of Chemical Technology
Beijing 100029 (China)

Y. Bai,[+] Dr. J. Liu, Prof. X.-D. Wen
Institute of Coal Chemistry, Chinese Academy of Sciences
Taiyuan 030001 (China)
and
Synfuels China
Beijing 100195 (China)

Dr. J. Liu
College of Chemistry and Environmental Science, Inner Mongolia Key Laboratory of Green Catalysis, Inner Mongolia Normal University
Hohhot 010022 (China)

Dr. W. Wang
Key Laboratory of Photochemistry, Institute of Chemistry, Chinese Academy of Sciences
Beijing 100190 (China)

Dr. B. Yang, Prof. Q. Dai
CAS Key Laboratory of Nanophotonic Materials and Devices, CAS Key Laboratory of Standardization and Measurement for Nanotechnology, CAS Center for Excellence in Nanoscience, National Center for Nanoscience and Technology
Beijing 100190 (China)

Prof. G. I. N. Waterhouse
School of Chemical Sciences, The University of Auckland
Auckland 1142 (New Zealand)

[+] These authors contributed equally to this work.

ing water and efficiently driving the WGSR with clean energy at low temperatures is a priority.

Recently, it was reported that the WGSR could be driven by semiconductor photocatalysts under light irradiation at room temperature.[5] However, whilst of fundamental interest, the rates of hydrogen production in the photocatalytic WGSR studies are far below industry levels.[5a–d] In contrast, Cu-based photothermal WGSR catalysts (CuO_x semiconductors) operating at 250–350 °C under light irradiation yielded H_2 production rates close to traditional high-temperature thermal catalysts.[5e–g,6] However, the performance of these photothermal WGSR catalysts at lower temperatures (< 250 °C) was inferior to thermal nobel metal-based catalysts.[2,7] By exploiting the localised surface plasmon resonance (LSPR) effects in metal nanoparticle-based catalysts (Au, Ag and Cu), it may be possible to significantly lower the operating temperature of the WGSR.[8] Hot electrons generated from the copper nanoparticles under LSPR excitation can be transferred to adsorbates such as water, thereby leading to enhanced adsorbate activation.[9] By this approach, it should be possible to overcome the high barrier of water dissociation to *OH and *H, leading to enhanced WGSR activity under very mild conditions.[10] To date, Cu LSPR effects have not been exploited in low-temperature WGSR studies, motivating a detailed investigation. The topological transformation method using layered double hydroxide (LDH) nanosheets as a precursor offers many advantages in the synthesis of supported metal nanoparticle catalysts, including high metal loading capacity, high metal dispersion and small size of the active metal particles.[11] We hypothesized that by using a CuAl-containing LDH precursor, it should be possible to synthesize catalysts with densely packed Cu nanoparticles on a two-dimensional (2D) alumina support, thus achieving efficient photo-driven low-temperature WGSR catalysis.

Herein, we synthesized a novel LDH-derived copper-based catalyst (LD-Cu) for the photo-driven WGSR, comprising Cu nanoparticles dispersed in high density over an amorphous alumina support. Under UV/Vis irradiation from a Xe lamp, LD-Cu demonstrated excellent H_2 production activity at low temperatures (160–240 °C), with notably enhanced WGSR activity compared to tests under dark conditions. WGSR tests under different monochromatic light sources revealed the elevated H_2 production activity under UV/Vis irradiation was due to excitation of the LSPR of the Cu nanoparticles leading to the creation of hot electrons. In situ diffuse reflectance Fourier transform infrared spectroscopy (DRIFTS) and density functional theory (DFT) calculations further revealed that light-induced LSPR effects promoted the activation of water and the generation of hydrogen. To our knowledge, this is the first study to report a significant improvement of WGSR performance through Cu LSPR effects. Results pave the way for the development of low-cost photo-driven Cu catalyst systems for the WGSR and other low-temperature photothermal reactions.

Results and Discussion

For the synthesis of the LD-Cu catalyst (Figure 1a), CuAl layered double hydroxide nanosheets (CuAl-LDH) with a Cu/Al ratio of 1:1 was firstly prepared, then calcined to form a CuAl-mixed metal oxide (CuAl-MMO) at 500 °C. Thermal reduction of the CuAl-MMO in a H_2/Ar (10/90, v/v) atmosphere at 200 °C (the reduction temperature was determined according to the H_2-TPR profile in Figure S1) yielded LD-Cu. Owing to the 2D layered structure of the CuAl-LDH precursor (shown in Figure S2), the obtained CuAl-MMO and LD-Cu products also possessed two-dimensional morphologies (Figure S3 and S4a), consistent with the topotactic transformation of the LDH nanosheets.[12] High angle annular dark field-scanning transmission electron microscopy (HAADF-STEM) imaging and element maps showed Cu nanoparticles densely distributed over an alumina support (Figure 1b). High-resolution transmission electron microscopy (HRTEM) further confirmed the presence of Cu nanoparticles highly dispersed on alumina, with the average size of the Cu nanoparticles estimated to be 7.1 ± 1.2 nm (Figure S4b). Lattice fringes with a spacing of 0.21 nm, corresponding to Cu (111) planes (Figure 1c), further verified the presence of metallic Cu nanoparticles. Energy dispersive spectrometry (EDS) analysis showed that the Cu/Al ratio of LD-Cu was still $\approx 1:1$ (Figure S5), the same as the CuAl-LDH precursor (See Experimental Procedures for details). Inductively coupled plasma-optical emission spectroscopy (ICP-OES) and N_2O titration tests were conducted to further confirm the catalyst composition and Cu dispersion of LD-Cu, respectively (Table S1). X-ray diffraction (XRD) was used to track the structural changes on going from CuAl-LDH to CuAl-MMO and finally LD-Cu (Figure S6). CuAl-LDH showed a characteristic set of (003), (006) and (009) reflections, which were replaced by reflections due to metallic Cu nanoparticles in LD-Cu. Cu *K*-edge X-ray absorption spectroscopy (XAS) was also applied to follow the topotactic structural transformation of CuAl-LDH to LD-Cu (Figure 1d). The Cu *K*-edge X-ray absorption near-edge structure (XANES) spectra for CuAl-LDH and CuAl-MMO were similar to that of CuO, confirming the presence of Cu^{2+} coordinated by oxygen. Conversely, the Cu *K*-edge XANES data for LD-Cu resembled that of the metallic Cu foil reference, indicating the transformation of cationic Cu species to metallic Cu during the CuAl-MMO reduction step. Cu *K*-edge extended X-ray absorption fine structure (EXAFS) results supported this conclusion (Figure 1e). The EXAFS data for CuAl-LDH and CuAl-MMO showed an intense Cu–O coordination feature at ≈ 1.5 Å in R space, whereas LD-Cu only showed metallic Cu–Cu coordination (2.2 Å in R space). In k space (Figure S7), LD-Cu showed a main oscillation due to metallic Cu at 6.5 $Å^{-1}$ whereas CuAl-LDH and CuAl-MMO showed a main oscillation due to cationic Cu at 4.0 $Å^{-1}$. Based on the results above, it can be concluded that the stepwise transformation CuAl-LDH→CuAl-MMO→LD-Cu created a catalyst with a dense loading of small Cu nanoparticles supported on amorphous Al_2O_3.

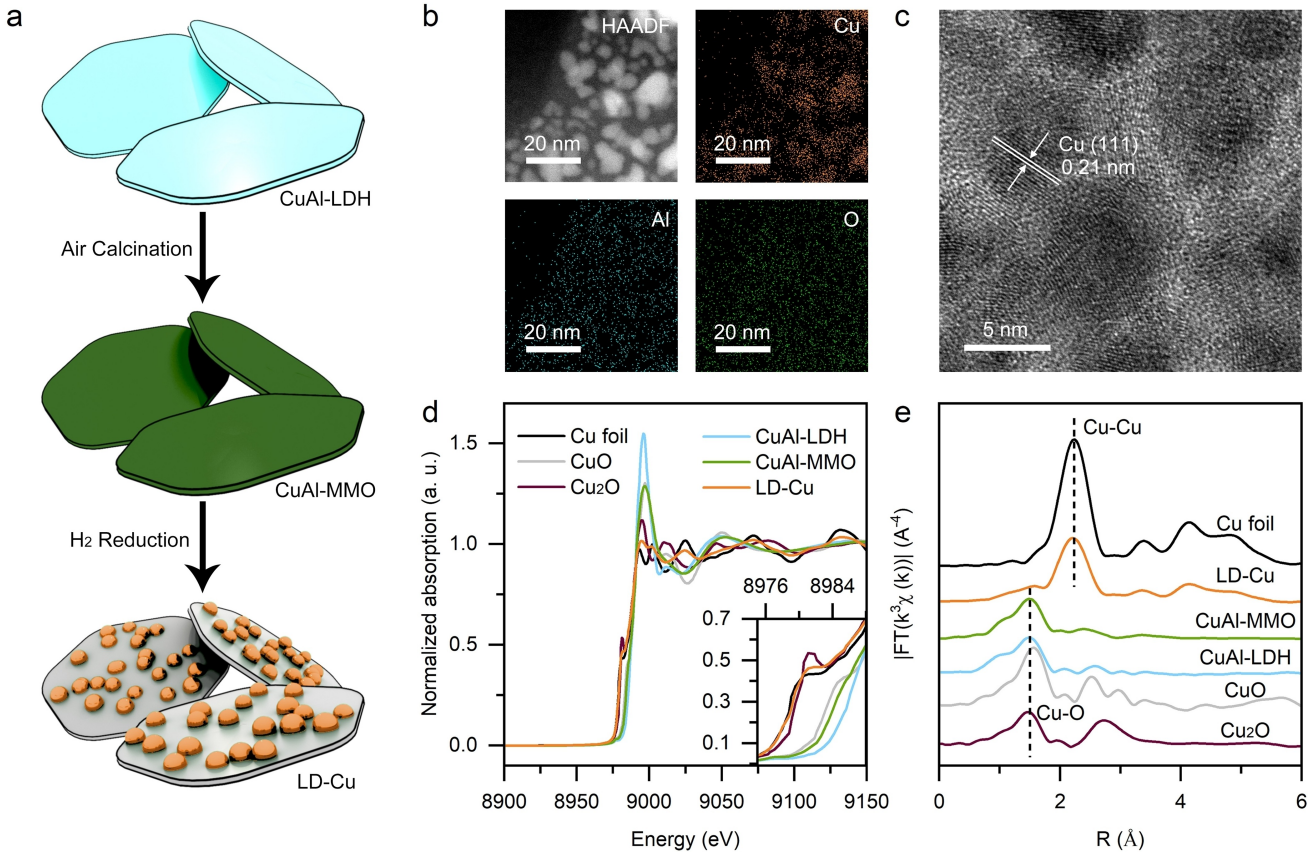

Figure 1. a) Synthesis of LD-Cu from CuAl-LDH nanosheets; b) HAADF-STEM image and EDS element maps for LD-Cu; c) HRTEM image for LD-Cu; d) Cu *K*-edge XANES and e) Cu *K*-edge EXAFS spectra in R space for CuAl-LDH, CuAl-MMO, LD-Cu and selected reference samples.

The obtained LD-Cu catalyst showed excellent light absorption at UV and visible wavelengths, thus suggesting the catalyst would possess good photothermal efficiency (Figure S8). Under UV/Vis irradiation with a light intensity of 1.4 W cm^{-2}, the temperature of LD-Cu surface increased rapidly to 200 °C over 15 min and then maintained this temperature (Figure S9). Figure 2a examines the photo-driven WGSR performance of LD-Cu under UV/Vis irradiation at mild temperatures between 160 to 240 °C. The H_2 production rate over LD-Cu at 200 °C was a remarkable 114.35 μmol g_{cat}^{-1} s^{-1} under UV/Vis irradiation with the light intensity of 1.4 W cm^{-2}. In the tested temperature window, the photo-driven WGSR offered significantly higher H_2 production rates than during thermal catalysis at the same temperature, indicating photo-driven promotion of the WGSR at these low temperatures. Furthermore, the apparent activation energy for the WGSR decreased from 35.3 kJ mol^{-1} under thermal conditions to 27.3 kJ mol^{-1} under UV/Vis irradiation conditions (Figure 2b). Importantly, the H_2 production at 200 °C showed a strong dependence on the UV/Vis light intensity (Figure 2c), further suggesting that the enhanced WGSR activity under UV/Vis irradiation originated from LSPR effects (i.e. hot electron injection from the Cu nanoparticles into H_2O and CO reactants).[8] The WGSR performance of previously reported photo-driven and thermal catalytic systems are summarized in Figure 2d and Table S2, with the various catalysts being compared on the basis of their mass specific activity. The comparison reveals that the LD-Cu catalyst developed in this work operated at a much lower WGSR temperature compared with the previously reported photothermal catalysts based on Cu-containing semiconductors. Moreover, the performance of LD-Cu was similar to noble metal-based catalysts in thermo-catalysis, significantly better than the traditional thermo-catalytic Cu-based catalysts (including a commercial $Cu/ZnO/Al_2O_3$ catalyst), and also vastly superior to photocatalytic materials operating at room temperature. LD-Cu showed a low WGSR activation energy and a low WGSR temperature window (Figure 2e), confirming that the photo-driven strategy adopted here allowed efficient activation of reactant molecules (H_2O and CO).[2a,b,6b,c,7b–d,13] Next, photo-driven WGSR was conducted for 5 cycles over the LD-Cu catalyst, with the results shown in Figures S10–12.

To investigate the specific promotion mechanism(s) occurring on LD-Cu under UV/Vis irradiation leading to the enhanced low-temperature WGSR performance, we conducted a series of fundamental studies combining in situ experiments and theoretical simulations. We first measured the WGSR activity at 200 °C over LD-Cu under different "monochromatic" light irradiation in the UV/Vis range using different narrow bandpass filters (350, 400, 450, 500,

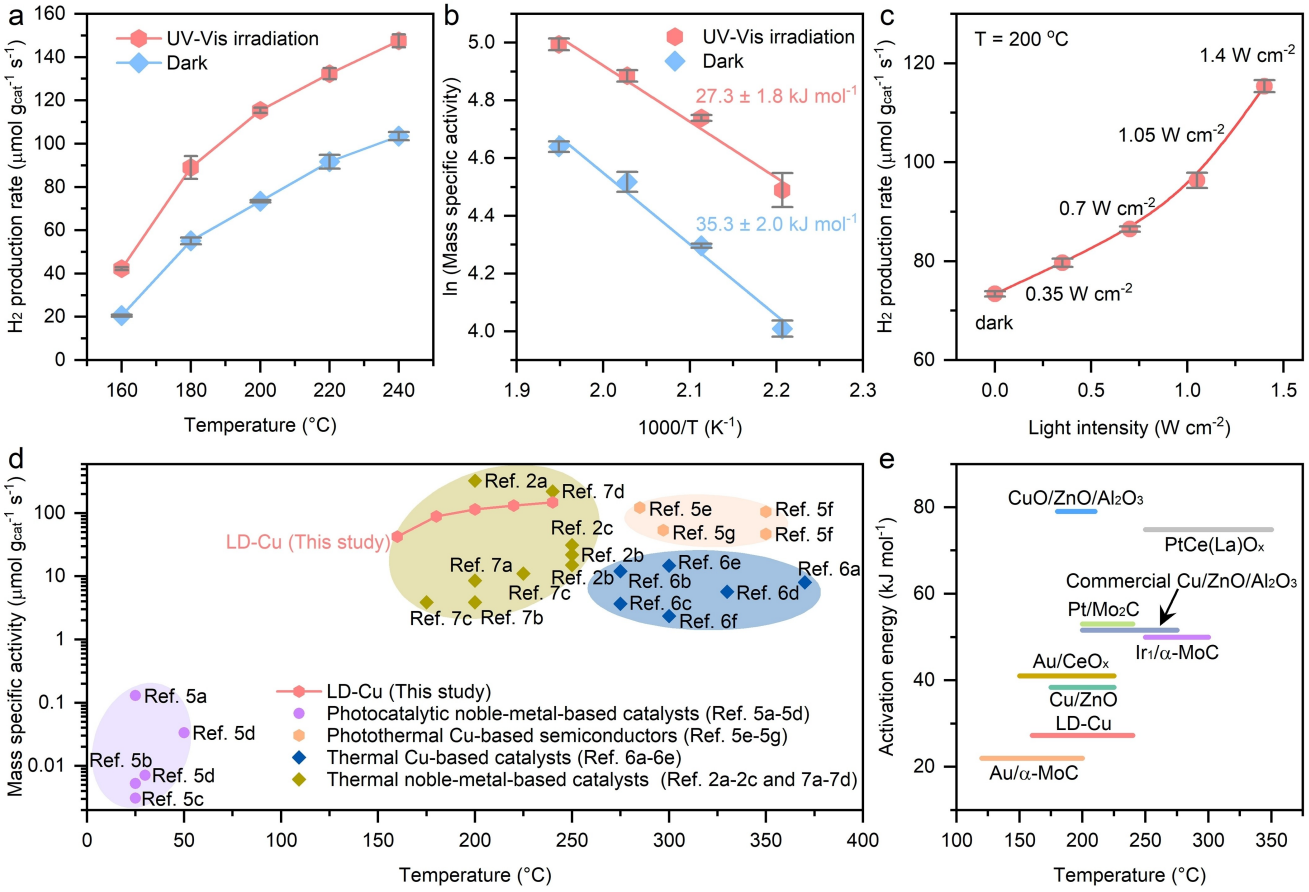

Figure 2. a) Comparison of H_2 production rates for photo-driven (UV/Vis irradiation) and thermal (Dark) WGSR over LD-Cu at 160–240 °C. b) Arrhenius plots of photo-driven (UV/Vis irradiation) and thermal (Dark) WGSR over LD-Cu. c) WGSR activity over LD-Cu at 200 °C and different UV/Vis light intensity. d) Summary of the mass specific activity for photothermal, thermal and photocatalytic WGSR over typical noble metal and Cu-based catalysts. e) WGSR activation energy of LD-Cu, typical noble metal and Cu-based catalysts.

550, 600 and 700 nm), as shown in Figure S13. WGSR activity was strongly dependent on the wavelength of the monochromatic light irradiation (Figure 3a). The maximum H_2 production rate was observed under 550 nm irradiation at a light intensity of 0.2 W cm^{-2} (comparable to the photo-driven performance under UV/Vis irradiation of 1.4 W cm^{-2}). As the wavelength of the excitation monochromatic light shifted further from 550 nm, the H_2 production rate decreased to the level of dark conditions. The Cu nanoparticles in LD-Cu showed a strong LSPR absorption at 550 nm (Figure S14), thus the H_2 production results in Figure 3a track closely with the LSPR excitation of the Cu nanoparticles. The light-to-energy storage (LES) efficiency calculated from the increased WGSR activity under monochromatic light irradiation at 550 nm was calculated to be 1.22 %. Indeed, the LES efficiency under different monochromatic light irradiation also tracked closely with the LSPR absorption of LD-Cu, further confirming that the generation of hot electrons by the Cu nanoparticles promoted the photo-driven WGSR. The enhanced kinetic isotope effect (KIE) is commonly used to study hot electron injection into the reactants (CO and H_2O) during plasmon-mediated photothermal processes.[14] Here, the KIE of D_2O was higher than that of ^{13}CO, indicating that plasmonic activation of H_2O was selectively enhanced on LD-Cu.[10] These studies further demonstrated that the LSPR effect of the supported Cu nanoparticles in LD-Cu boosted WGSR activity. To gain deeper insights about the LSPR effect, light-induced electric fields around single Cu nanoparticles and densely arranged Cu nanoparticles with the appropriate size were simulated by the finite difference time domain (FDTD) method. Under light irradiation at 550 nm, the maximum intensity ($|E|^2/|E_0|^2$) of the electric field around a supported Cu nanoparticle with the diameter of 8 nm was ≈21, as shown in Figure S15. For the LD-Cu nanocatalyst containing abundant Cu nanoparticles (Figure S16), the electric fields were strongly localized in the gaps between the neighboring Cu nanoparticles. Therefore, the maximum intensity of the electric field over LD-Cu in Figure 3c and 3d was much higher (≈62) than that around a single supported Cu nanoparticle. The results suggest that the visible-light absorbing Cu nanoparticles in LD-Cu acted as the hot electron source and active sites in the WGSR, unlike Ouyang et al.'s work where UV absorption by CuO_x semiconductors created conduction band electrons which then participated in the WGSR.[5e]

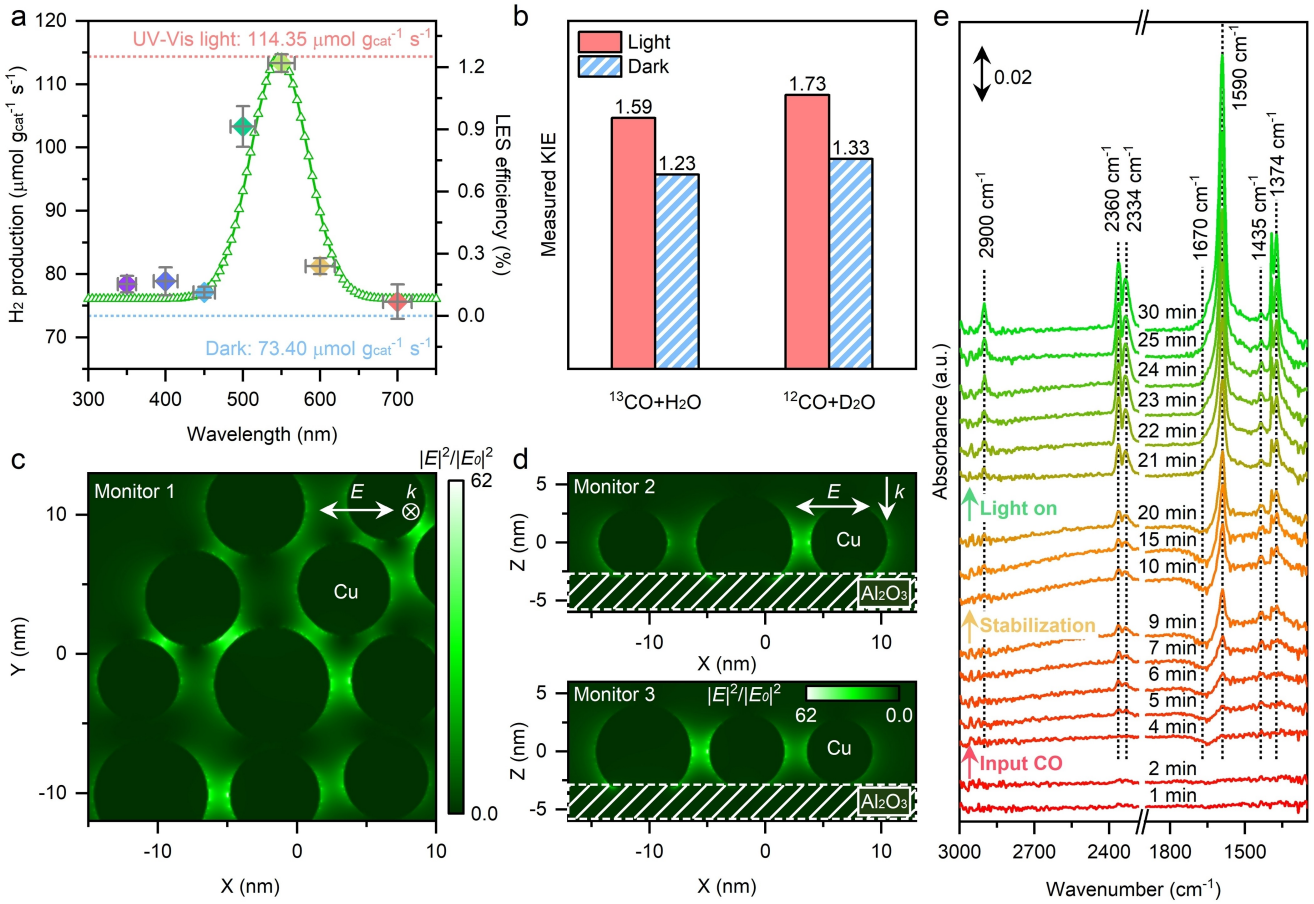

Figure 3. a) WGSR activity and LES efficiency over the LD-Cu catalysts at 200 °C under irradiation of different light wavelengths. The green curve is the absorption spectrum for a Cu nanoparticle showing the LSPR excitation. b) KIE comparison between light and dark conditions over LD-Cu at 200 °C. c, d) Simulated electric fields according to the actual distribution of Cu nanoparticles supported on Al_2O_3. The colored bar shows the electric field intensity normalized by the light source intensity ($|E|^2/|E_0|^2$). e) In situ DRIFT spectra of LD-Cu for WGSR under dark and light conditions at 200 °C.

In order to explore the influence of LSPR-mediated hot electrons on the WGSR intermediates, in situ DRIFTS data were collected on LD-Cu under a flowing gas (Ar or CO) containing water vapor at 200 °C (Figure 3e). Initially adsorption/reaction studies were conducted in the dark. At the beginning of the experiments, argon gas with water vapor was passed over the catalyst. After 2 min, the Ar was swapped for CO, with the intensity of the O–H bending vibration of adsorbed water (*H_2O) at around 1670 cm^{-1} decreasing rapidly (becoming negative due to the consumption of water), indicating the occurrence of the thermal WGSR.[15] The consumption of *H_2O was due to its reforming with *CO to produce adsorbed carboxyl groups (*COOH) as the crucial WGSR intermediate.[3a] The carboxyl groups could easily dehydrogenate over metal sites to form carboxylate groups (*COO^-), leading to the intensification of peaks at 1590 and 1374 cm^{-1} associated with anti-symmetric and symmetric stretching O–C-O vibrations complexed with surface Cu centers, respectively.[16] The subsequent formation of *CO_2 was later evidenced by the appearance of additional peaks at around 2360 and 2334 cm^{-1}), confirming that the WGSR proceeded via a carboxyl mechanism over LD-Cu. After the introduction of CO, the peak intensities for the *COO^- and *CO_2 features remained unchanged after ≈10 min, indicating that the absorption and activation of water over the catalyst surface was limiting the further generation of *COO^- intermediates and final products (*CO_2) in thermal WGSR (under dark conditions). When monochromatic laser light at 532 nm was irradiated on the catalyst surface, the negative peak for *OH groups at around 1670 cm^{-1} disappeared, indicating that the adsorption and activation of water was promoted on the plasmonic LD-Cu catalysts under light irradiation. Moreover, the peak intensities for the *COO^- intermediate (1590 and 1374 cm^{-1}) and *CO_2 product (2360 and 2334 cm^{-1}) increased rapidly, indicating that the additional surface *OH groups enhanced WGSR activity. Further, a new peak at around 2900 cm^{-1} appeared, which could readily be assigned to the C–H vibrations in formate (*HCOO) created through a CO_2 hydrogenation pathway (*CO_2+*H).[3a,17] It should be noted that under the dark conditions, a minor peak due to bicarbonate (1435 cm^{-1}, symmetric O–C-O stretching vibration) was observed, which lost intensity under 532 nm irradiation. This suggested that

the desorption of CO_2 was promoted in the photo-driven regime, thus preventing bicarbonate formation.[18] No other new peaks were observed, indicating that the hot electrons created by Cu nanoparticles in the plasmonic LD-Cu catalysts did not change the main reaction path or produce any new intermediates, but simply promoted the original carboxyl reaction mechanism by overcoming the high barriers of water activation and dissociation. Figure S17 shows the integrated peak intensities for the different groups ($*H_2O$, $*COO^-$ and $*CO_2$) with time during the in situ DRIFTS experiment under dark and light conditions. Note the abrupt change in the peak intensities cause by the application of the 532 nm laser after 20 min. These results confirmed that the hot electrons induced by LSPR over LD-Cu enhanced the adsorption and activation of water, thus promoting the production of carboxyl intermediates and enhancing WGSR kinetics under light irradiation.

Finally, to obtain full understanding of reaction mechanism, conventional DFT (ground state) and constrained DFT (excited state) calculations were preformed to study the effect of light irradiation on potential energy surface of the WGSR via the carboxyl pathway.[19] The computational details are provided in the Experimental Procedures. A Cu (111) surface model was used in the calculations (Figure S18). Since the Cu nanoparticles are the active site for the WGSR, it was not necessary to include the alumina support in the calculations. The route is initiated by $*H_2O$ activation to yield *OH and *H species. Then *CO reacts with *OH species to produce the final $*CO_2$ product, with *H species combining to produce H_2. The calculated reaction energies and energy barriers for different elementary reaction steps on the Cu (111) surface were listed in Table S3, with the corresponding transition state (TS) configurations shown in Figure S19. According to our calculations (Figure 4a), electron excitation had a negligible effect on the adsorption strength of both $*H_2O$ and *CO. But for the activation of $*H_2O$ through O–H bond cleavage ($*H_2O \rightarrow *H+*OH$), the activation barrier was greatly decreased (0.63 eV under excited state conditions vs. 1.05 eV under ground state conditions). This is consistent with our experimental observation that LSPR excitation processes in LD-Cu promoted water dissociation. Thermodynamically, the $*H_2O \rightarrow *H+*OH$ step was also favorable under excited state conditions (an exothermic energy release of 0.33 eV compared to only 0.06 eV under ground state conditions). For the subsequent *COOH formation and *COOH dissociation to $*CO_2$ steps, though the reaction barriers were slightly increased in the excited state, though the overall potential energy profile was downshifted and thus more energetically favorable compared to the ground state. In addition, the hydrogen evolution reaction via the combination of two hydrogen atoms ($*H+*H \rightarrow *H_2$) was favored kinetically (0.44 vs. 0.85 eV) and thermodynamically (0.30 vs. 0.41 eV) under the excited electron regime. The excited state also allowed easier desorption of the products (H_2 and CO_2) with stronger exothermic energies compared to the ground state (0.12 vs. 0.03 eV). We further considered the role of metal-oxide interface in the WGSR (Figure S20), which demonstrated that the overall potential energy profile on a Cu/Al_2O_3 interface under excited state conditions was downshifted and thus energetically favorable compared to that under ground state conditions, exactly the same trend as was seen for the Cu(111) model surface. In summary, both the activation of H_2O and the generation of H_2 were promoted in the presence of excited electrons. In Figure 4b, we propose a LSPR-mediated WGSR mechanism over LD-Cu in which the light-induced LSPR electrons promote the dissociation of H_2O, leading to the generation of H_2 and CO_2 through a carboxyl intermediate pathway.

Conclusion

In conclusion, a LD-Cu catalyst with a high density of Cu nanoparticles was successfully synthesized from a CuAl-LDH nanosheet precursor and a CuAl-MMO intermediate. The LD-Cu catalyst exhibited a very low WGSR reaction temperature window and excellent activity for H_2 production under UV/Vis irradiation compared to the dark (thermal) conditions. Detailed experimental and theoretical

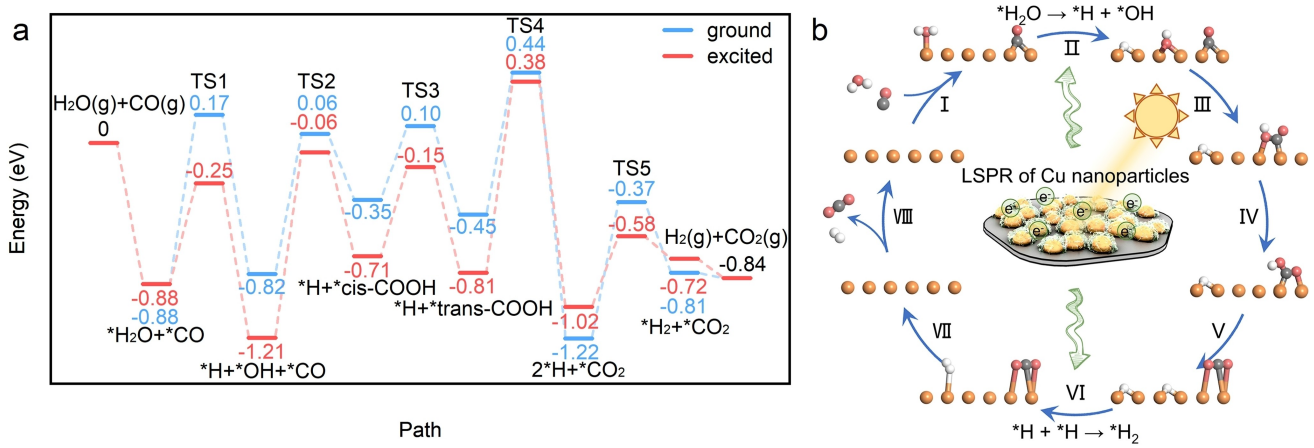

Figure 4. a) The ground-state and excited-state potential energy profile of the WGSR on a Cu (111) surface. b) Proposed photo-driven WGSR mechanism through a carboxyl pathway over the LD-Cu catalyst. Color code of atoms: Cu (orange), C (grey), O (red), H (white).

investigations, including in situ DRIFTS characterization studies and DFT calculations, revealed that the Cu nanoparticle LSPR effect created hot electrons which selectively promoted the dissociation of $*H_2O$ and the combination of two *H, thereby enhancing the kinetics of H_2 and CO_2 evolution via a carboxyl pathway. This work demonstrates for the first time that plasmonic Cu nanoparticle-based catalysts can efficiently drive the WGSR at very low temperatures, thus opening new vistas for the design of low-cost photo-driven catalysts for the WGSR and other catalytic reactions that rely on water activation to proceed efficiently.

Acknowledgements

The authors are grateful for financial support from the National Key Projects for Fundamental Research and Development of China (2018YFB1502002), the National Natural Science Foundation of China (51825205, 52120105002, 22088102, 21902168), the Postdoctoral Science Foundation of China (2021M703288), the Beijing Natural Science Foundation (2191002), the CAS Project for Young Scientists in Basic Research (YSBR-004), the DNL Cooperation Fund, CAS (DNL202016), the Youth Innovation Promotion Association of the CAS, and the Collaborative Innovation Center for Water Environment Security of Inner Mongolia Autonomous Region, China (XTCX003). The XAS experiments were conducted in 1 W1B beamline of Beijing Synchrotron Radiation Facility (BSRF). GINW is supported by a James Cook Research Fellowship, administered by the Royal Society Te Apārangi. This work received additional financial support from the MacDiarmid Institute for Advanced Materials and Nanotechnology and the Energy Education Trust of New Zealand.

Conflict of Interest

The authors declare no conflict of interest.

Data Availability Statement

Research data are not shared.

Keywords: Cu-Based Catalysts · Layered Double Hydroxide · Localized Surface Plasmon Resonances · Photo-Driven Catalysis · Water-Gas Shift Reaction

[1] a) T. Takata, J. Jiang, Y. Sakata, M. Nakabayashi, N. Shibata, V. Nandal, K. Seki, T. Hisatomi, K. Domen, *Nature* **2020**, *581*, 411–414; b) Y. Li, Y.-K. Peng, L. Hu, J. Zheng, D. Prabhakaran, S. Wu, T. J. Puchtler, M. Li, K.-Y. Wong, R. A. Taylor, S. C. E. Tsang, *Nat. Commun.* **2019**, *10*, 4421.

[2] a) S. Yao, X. Zhang, W. Zhou, R. Gao, W. Xu, Y. Ye, L. Lin, X. Wen, P. Liu, B. Chen, E. Crumlin, J. Guo, Z. Zuo, W. Li, J. Xie, L. Lu, C. J. Kiely, L. Gu, C. Shi, J. A. Rodriguez, D. Ma, *Science* **2017**, *357*, 389–393; b) Q. Fu, H. Saltsburg, M. Flytzani-Stephanopoulos, *Science* **2003**, *301*, 935–938; c) K. Ding, A. Gulec, M. Johnson Alexis, M. Schweitzer Neil, D. Stucky Galen, D. Marks Laurence, C. Stair Peter, *Science* **2015**, *350*, 189–192.

[3] a) A. A. Gokhale, J. A. Dumesic, M. Mavrikakis, *J. Am. Chem. Soc.* **2008**, *130*, 1402–1414; b) Y.-L. Lee, K. Lee, C. H. Ko, H.-S. Roh, *Chem. Eng. J.* **2022**, *431*, 134299.

[4] X. Zhang, M. Zhang, Y. Deng, M. Xu, L. Artiglia, W. Wen, R. Gao, B. Chen, S. Yao, X. Zhang, M. Peng, J. Yan, A. Li, Z. Jiang, X. Gao, S. Cao, C. Yang, A. J. Kropf, J. Shi, J. Xie, M. Bi, J. A. van Bokhoven, Y.-W. Li, X. Wen, M. Flytzani-Stephanopoulos, C. Shi, W. Zhou, D. Ma, *Nature* **2021**, *589*, 396–401.

[5] a) F. Sastre, M. Oteri, A. Corma, H. García, *Energy Environ. Sci.* **2013**, *6*, 2211–2215; b) S. M. Fang, B. H. Chen, J. M. White, *J. Phys. Chem.* **1982**, *86*, 3126–3130; c) L. Millard, M. Bowker, *J. Photochem. Photobiol. A* **2002**, *148*, 91–95; d) C. Yixuan, W. Zhaobin, C. Yanxin, L. Huaxin, H. Zupei, L. Huiqing, D. Yonglei, Y. Chuying, L. Wenzhao, *J. Mol. Catal.* **1983**, *21*, 275–289; e) L. Zhao, Y. Qi, L. Song, S. Ning, S. Ouyang, H. Xu, J. Ye, *Angew. Chem. Int. Ed.* **2019**, *58*, 7708–7712; *Angew. Chem.* **2019**, *131*, 7790–7794; f) F. Liu, L. Song, S. Ouyang, H. Xu, *Catal. Sci. Technol.* **2019**, *9*, 2125–2131; g) C. Shi, D. Yuan, L. Ma, Y. Li, Y. Lu, L. Gao, X. San, S. Wang, G. Fu, *J. Mater. Chem. A* **2020**, *8*, 19467–19472.

[6] a) M. Zhu, P. Tian, R. Kurtz, T. Lunkenbein, J. Xu, R. Schlögl, I. E. Wachs, Y.-F. Han, *Angew. Chem. Int. Ed.* **2019**, *58*, 9083–9087; *Angew. Chem.* **2019**, *131*, 9181–9185; b) Z. H. Zhang, S. S. Wang, R. Song, T. Cao, L. F. Luo, X. Y. Chen, Y. X. Gao, J. Q. Lu, W. X. Li, W. X. Huang, *Nat. Commun.* **2017**, *8*, 488; c) Z. Zhang, X. Chen, J. Kang, Z. Yu, J. Tian, Z. Gong, A. Jia, R. You, K. Qian, S. He, B. Teng, Y. Cui, Y. Wang, W. Zhang, W. Huang, *Nat. Commun.* **2021**, *12*, 4331; d) M. Zhu, I. E. Wachs, *ACS Catal.* **2016**, *6*, 1764–1767; e) F. R. García-García, M. A. Rahman, I. D. González-Jiménez, K. Li, *Catal. Today* **2011**, *171*, 281–289; f) G. Aguila, A. Valenzuela, S. Guerrero, P. Araya, *Catal. Commun.* **2013**, *39*, 82–85.

[7] a) N. Liu, M. Xu, Y. Yang, S. Zhang, J. Zhang, W. Wang, L. Zheng, S. Hong, M. Wei, *ACS Catal.* **2019**, *9*, 2707–2717; b) L. Sun, J. Xu, X. Liu, B. Qiao, L. Li, Y. Ren, Q. Wan, J. Lin, S. Lin, X. Wang, H. Guo, T. Zhang, *ACS Catal.* **2021**, *11*, 5942–5950; c) N. Yi, R. Si, H. Saltsburg, M. Flytzani-Stephanopoulos, *Energy Environ. Sci.* **2010**, *3*, 831–837; d) N. M. Schweitzer, J. A. Schaidle, O. K. Ezekoye, X. Pan, S. Linic, L. T. Thompson, *J. Am. Chem. Soc.* **2011**, *133*, 2378–2381.

[8] a) L. Zhou, J. M. P. Martirez, J. Finzel, C. Zhang, D. F. Swearer, S. Tian, H. Robatjazi, M. Lou, L. Dong, L. Henderson, P. Christopher, E. A. Carter, P. Nordlander, N. J. Halas, *Nat. Energy* **2020**, *5*, 61–70; b) P. Christopher, H. Xin, A. Marimuthu, S. Linic, *Nat. Mater.* **2012**, *11*, 1044–1050.

[9] a) X. Xu, F. Luo, W. Tang, J. Hu, H. Zeng, Y. Zhou, *Adv. Funct. Mater.* **2018**, *28*, 1804055; b) Y. Xin, K. Yu, L. Zhang, Y. Yang, H. Yuan, H. Li, L. Wang, J. Zeng, *Adv. Mater.* **2021**, *33*, 2008145.

[10] S. Xu, S. Chansai, C. Stere, B. Inceesungvorn, A. Goguet, K. Wangkawong, S. F. R. Taylor, N. Al-Janabi, C. Hardacre, P. A. Martin, X. Fan, *Nat. Catal.* **2019**, *2*, 142–148.

[11] M. Xu, M. Wei, *Adv. Funct. Mater.* **2018**, *28*, 1802943.

[12] a) Z. Li, J. Liu, Y. Zhao, G. I. N. Waterhouse, G. Chen, R. Shi, X. Zhang, X. Liu, Y. Wei, X.-D. Wen, L.-Z. Wu, C.-H. Tung, T. Zhang, *Adv. Mater.* **2018**, *30*, 1800527; b) Y. Zhao, Z. Li, M. Li, J. Liu, X. Liu, G. I. N. Waterhouse, Y. Wang, J. Zhao, W. Gao, Z. Zhang, R. Long, Q. Zhang, L. Gu, X. Liu, X. Wen, D. Ma, L.-Z. Wu, C.-H. Tung, T. Zhang, *Adv. Mater.* **2018**, *30*, 1803127; c) Z. Li, J. Liu, Y. Zhao, R. Shi, G. I. N. Waterhouse, Y. Wang, L.-Z. Wu, C.-H. Tung, T. Zhang, *Nano Energy* **2019**, *60*, 467–475; d) X. Zhang, G. Q. Cui, H. S. Feng, L. F. Chen, H.

Wang, B. Wang, X. Zhang, L. R. Zheng, S. Hong, M. Wei, *Nat. Commun.* **2019**, *10*, 5812.
[13] N. A. Koryabkina, A. A. Phatak, W. F. Ruettinger, R. J. Farrauto, F. H. Ribeiro, *J. Catal.* **2003**, *217*, 233–239.
[14] S. Yu, P. K. Jain, *Angew. Chem. Int. Ed.* **2020**, *59*, 22480–22483; *Angew. Chem.* **2020**, *132*, 22666–22669.
[15] X. Chen, G. He, Y. Li, M. Chen, X. Qin, C. Zhang, H. He, *ACS Catal.* **2020**, *10*, 9706–9715.
[16] a) J. Vecchietti, A. Bonivardi, W. Xu, D. Stacchiola, J. J. Delgado, M. Calatayud, S. E. Collins, *ACS Catal.* **2014**, *4*, 2088–2096; b) K. Mudiyanselage, S. D. Senanayake, L. Feria, S. Kundu, A. E. Baber, J. Graciani, A. B. Vidal, S. Agnoli, J. Evans, R. Chang, S. Axnanda, Z. Liu, J. F. Sanz, P. Liu, J. A. Rodriguez, D. J. Stacchiola, *Angew. Chem. Int. Ed.* **2013**, *52*, 5101–5105; *Angew. Chem.* **2013**, *125*, 5205–5209.
[17] M. Xu, S. Yao, D. Rao, Y. Niu, N. Liu, M. Peng, P. Zhai, Y. Man, L. Zheng, B. Wang, B. Zhang, D. Ma, M. Wei, *J. Am. Chem. Soc.* **2018**, *140*, 11241–11251.
[18] N. C. Nelson, M.-T. Nguyen, V.-A. Glezakou, R. Rousseau, J. Szanyi, *Nat. Catal.* **2019**, *2*, 916–924.
[19] B. Kaduk, T. Kowalczyk, T. Van Voorhis, *Chem. Rev.* **2012**, *112*, 321–370.

Manuscript received: December 30, 2022
Accepted manuscript online: February 3, 2023
Version of record online: February 17, 2023